Pressure wave focusing effects following laser medical procedures in human eyes

D. Horvat[1] · T. Požar[1] · B. Starman[1] · M. Halilovič[1] · R. Petkovšek[1]

Abstract

Comparative analysis of pressure wave propagation, following laser-induced ablation of the human cornea, was performed. Evolution of the pressure field as well as temporal and spatial dependencies of the transient pressure amplitudes created at various input laser parameters, corresponding to different typical procedures of laser eye surgery, is presented comprehensively. The computations were performed with the next generation of the acoustic eye model, previously validated against existing measurements. The analysis allows the assessment of potentially problematic regions within the eye where the resultant positive and/or negative pressure may exceed values which are considered safe for the patient.

Keywords Shock waves · Photoablation · Laser ultrasonics · Cavitation · Acoustic focusing · Negative pressure

1 Introduction

At present, various conventional refraction-correcting laser procedures as well as custom-guided visual acuity treatments are clinically available. The procedures involve photoablation of corneal tissue using UV laser pulses. From the first clinical study in 1988 [1], modern laser refractive surgery is advancing in the development of customized ablation profiles, to treat higher-order aberrations and to not induce new ones. The first three generations of excimer laser systems had used broad excimer laser beam, which were later followed by more advanced systems involving small, "flying spot" laser beams featuring customized wavefront generation, faster ablation rate, sophisticated tracking systems using smaller laser beam spot sizes to achieve better lateral photoablation resolution, etc., overall resulting in a better outcome of the treatment [2]. Despite these advances, broad beam photoablation technology is still being sold and used today.

✉ T. Požar
tomaz.pozar@fs.uni-lj.si

1 Faculty of Mechanical Engineering, University of Ljubljana, Aškerčeva 6, 1000 Ljubljana, Slovenia

The photoablation of cornea involves ejection of corneal tissue. As a compensation, this ejection gives rise to a reaction force which generates a transient compression, starting as a shock wave, propagating through the eye tissues as a high-pressure acoustic pulse. Because of the concave spherical shape of the cornea, the wavefront generated by larger beams is focused inside the eye. Additionally, due to complex geometrical characteristics and material properties of the eye tissues, the wave evolution during its propagation is difficult to describe analytically, because it involves reflections at boundaries between different tissues, attenuation and phase shift. The location of the focal volume and the depth of focus depend both on the propagation characteristics and on the size and spatiotemporal shape of the source. When focused, the pressure amplitude may well surpass the threshold for the potentially tissue damaging effects [3–7]. From the standpoint of tissue damage, the negative pressure (rarefactional waves) presents larger risk than the positive (compressional waves) [4].

This paper presents the dynamics of the pressure wave focusing inside the eye for the selected cases which correspond to different laser beam parameters, typically used in different contemporary medical procedures, such as LASIK (laser-assisted in situ keratomileusis) [8] or PRK (photorefractive keratectomy) [9]. Since in vivo measurements of transient acoustic pressure profiles in human eyes generated by photoablation have so far not been carried out, we have, based on the review of the existing

literature on experiments and theoretical approaches, developed a computer-based acoustic eye model (AEM) [3] which gives numerical estimates of spatial and temporal evolution of the pressure fields. This model was first validated [10] by comparison with existing, but scarce measurements of photoablation-induced pressure waveforms in ex vivo porcine and human eyes [11, 12], and then extended to incorporate other initial conditions. Here, the model is used to map the locations inside the eye where the highest pressure amplitudes, both positive and negative, are expected, with the aim to help medical professionals investigate the possible consequences of acoustic focusing within the human eye during the laser eye surgery. The pressure fields presented in this paper are the best scientific estimates currently at hand for the already approved refraction-correcting laser procedures. These results imply that when broad beams are used, negative pressure exceeds the threshold for acoustic cavitation (-200 bar [6]) in the vicinity of the acoustic focus which is located close or at the delicate membranes behind the ocular lens. The ophthalmic mechanical index of 0.23 (corresponding to -7.3 bar in our simulations), used as an index of cavitation bio-effects, is also surpassed by up to two orders of magnitude [13]. Since it has still not been proven if this acoustic focusing mechanism might be responsible for any short- or long-term complications of the posterior part of the lens, it should thus be thoroughly investigated by research ophthalmologists.

2 Acoustic eye model

The acoustic eye model (AEM) is a computer-based numerical model of a typical human eye which performs a computation of propagating pressure transients once the initial pressure distribution is input into the model as the initial condition. The geometry and acoustic parameters of various ocular tissues are given in [10]. For the photoablation case, the input into the model is a temporal and spatial distribution of pressure on the outer surface of the cornea. Table 1 presents four selected pressure input profiles which correspond to ablation of the cornea by: (1st column) a large, flattop broad beam of 6.5 mm diameter, (2nd column) an iris-apodized, medium size flattop broad beam of 3.0 mm diameter, (3rd column) a 1 mm diameter Gaussian flying spot beam and (4th column) a very small size Gaussian flying spot beam of 0.35 mm diameter. These profiles correspond to the typical clinical parameters provided by the contemporary lasers used for LASIK and PRK.

Laser beam spatial fluence profile on the cornea was transformed to spatial pressure profile on the cornea using an experimentally determined linear ratio of 0.5 bar/(mJ/cm^2) [11–15]. Gaussian beams were transformed directly, while a cosine taper was added to the flattop pressure profiles, since tapered pressure profiles give rise to simulated waveforms that have a much better match to the measured axial pressure waveforms [10]. For the purpose of comparison, the average fluence for all four pressure inputs was taken at its most commonly used clinical value of 175 mJ/cm^2, which is approximately four times above the photoablation threshold, where ablation

Table 1 The spatial and temporal characteristics of typical laser pulses used in LASIK and PRK and the corresponding characteristics of the pressure pulses, used as the input for the numerical model

	PHOTOABLATION APPROACH		
	PARAMETERS OF A TYPICAL CONTEMPORARY LASER BEAM		
	Variable broad beam	Flying spot	
Laser type	Excimer ArF	Excimer ArF	DPSS 5H
Wavelength (nm)	193	193	208 –213
Beam size – diameter (mm)	0.65 – 6.5	0.9 – 1.2	0.25 – 0.6
Shape	Flat top (variable size)	Gaussian	Gaussian
Average fluence (mJ/cm^2)	150 –200	150 –200	175 –180
Energy per pulse (mJ)	1 –100	2	0.2
	LIGHT PULSES USED IN THE MODEL		
Type	Flat top	Gaussian	
Spot size	Large	Medium	Small	Very small
Diameter (mm)	6.5	3.0	1.0	0.35
Max. fluence (mJ/cm^2)	175	175	350	350
Avg. fluence (mJ/cm^2)	175	175	175	175
Energy (mJ)	58	12	1.4	0.17
	PRESSURE PULSES USED AS THE INPUT INTO THE MODEL		
Type	Flat top + taper	Gaussian	
Max. pressure (bar)	86	86	172	172
Total diameter (mm)	8.0	4.5	1.0	0.35
Flat part (mm)	6.5	3.0	/	/
Cosine taper (mm)	0.75	0.75	/	/
Force (N)	360	96	6.8	0.83

is most efficient [16]. As for the temporal shape, the pressure pulse lasts longer than the laser pulse, since the recoil force of the ablated material is still acting on the cornea after the laser pulse has already ceased. The temporal profile of the pressure was thus taken from the work of Siano et al. [11] who measured the pressure profiles immediately below the corneal endothelium.

3 Numerical procedure

From computational viewpoint, a typical human eye can be considered as a fluid–structure system. In our acoustic eye model, we modeled different eye tissues as compressible, inviscid, nonflowing, attenuating liquid media, which is a simplification of the actual behavior. In the present analysis, only the essential parts of the eye are considered and geometric simplifications are made, for example, the eye is modeled as an axisymmetric problem.

3.1 Mathematical model

The mathematical model of the dynamic response is based on the pressure field distribution $p(r, t)$ which is modeled by the linear wave equation with attenuation:

$$\nabla^2 p(r, t) + \frac{2\alpha}{c} \frac{\partial p(r, t)}{\partial t} + \frac{1}{c^2} \frac{\partial^2 p(r, t)}{\partial t^2} = 0, \tag{1}$$

where r is the spatial coordinate, t is the time, ∇^2 is the Laplacian operator, c is the wave speed in the fluid and α denotes the acoustic attenuation coefficient. This equation also assumes small local mass density gradient and acoustic attenuation gradient. It also assumes small-amplitude displacements and velocities of the fluid particles and must be associated with the boundary conditions and the initial conditions prescribed on the computational domain [17]. As presented in the previous section, the spatiotemporal pressure profile is prescribed on the outer edge of the cornea, while at the other outermost boundaries, the normal acoustic displacement, expressed as $\partial p / \partial n$, is set to zero. Except for the time of initial loading, the outermost boundaries are stress free, which gives rise to wave reflections.

3.2 Finite element formulation for direct integration of transient dynamics

A standard finite element spatial discretization of the wave equation is based on a variational principle or the method of weighted residuals (Galerkin method), which yields a discretized finite element equation. After the assembly process, the following system of equations is obtained:

$$M\ddot{p}^{n+1} + C\dot{p}^{n+1} + Kp^{n+1} = 0, \tag{2}$$

where M, C and K are the structural mass, damping and stiffness matrices, respectively. At the end of each time interval $n+1$, the nodal values of the acoustic pressure p^{n+1} are sought by Newton–Raphson algorithm, once the Newmark-β method,

$$\ddot{p}^{n+1} = \frac{1}{\beta \Delta t^2} \left(p^{n+1} - p^n \right) - \frac{1}{\beta \Delta t} \dot{p}^n - \left(\frac{1}{2\beta} - 1 \right) \ddot{p}^n, \tag{3a}$$

$$\dot{p}^{n+1} = \dot{p}^n + \Delta t \left[(1 - \gamma) \ddot{p}^n + \gamma \ddot{p}^{n+1} \right], \tag{3b}$$

is employed in Eq. (2). The Newmark parameters are set to $\beta = 1/4$ and $\gamma = 1/2$ to avoid any unwanted numerical damping. To increase the accuracy of the simulations, the finite element mesh was refined to consist of more than 15 quadratic quadrilateral finite elements over the pressure wavefront. The finest element mesh size was 7.5 μm, and the time step was set to $\Delta t = 1.0$ ns. The numerical analyses were performed in the ABAQUS 6.16 finite element software (Simulia, Providence, RI, 2018).

4 Results and discussion

The evolution of the resulting pressure field is presented for the different cases of laser input parameters in the four animations (Online resources 1–4). To make the comparison between the different cases easier, the discrete logarithmic color scale for all the presented cases is the same. The legend in the animations and in the figures shows the positive values of the pressure (compression) in different shades of red, while the negative values (rarefaction) are represented in blue.

In the first animation (Online resource 1), containing the pressure field evolution for the largest spot diameter (6.5 mm, flattop), the structure of the transient field can be observed best. In the beginning, it resembles the field of a pulsed circular flat piston [18], consisting of two linearly superimposable contributions: (1) the central planar compressional wave (here, the wavefront is slightly curved to match the curvature of the cornea), propagating inside the cylindrical volume representing the geometrical shadow of the source at the surface and propagating away from the source, and (2) the so-called edge wave, emanating from the rim of the circular (piston) source in a hemi-toroidal fashion. The outer part of the edge wave has the same polarity (positive pressure, compression) as the central wave, while the inner portion has the opposite polarity (negative pressure, rarefaction), consistent with

the simplified theory [18]. The two contributions to the total field can be identified clearly at the beginning of the animation and tracked as they propagate through the eye structures. Because of the slightly curved surface of the source, the central portion of the wave is focused near the posterior part of the eye lens, extending toward the vitreous humor. As discussed in detail elsewhere [10], the central part of the wave which is originally a monopolar spherical compression, upon passing its own focus, undergoes the so-called Gouy phase shift of π and thus transforms to a rarefaction. Around the focus, the transformation is not discernible, because of the superposition with the edge wave which arrives approximately at the same time. As the two contributions propagate, they decouple again and when they have traveled to the posterior of the eye it becomes clear that on the axis the leading wave (compression) originates from what was originally the outer portion of the edge wave, while the rarefaction, which arrives after a short pause, comes from the π-shifted central part. The origin of the contributing parts of the wave can also be confirmed by observing the distance they had travelled. All along the propagation, small-amplitude reflections take place at boundaries of tissues having slightly different acoustic impedances. Following this description, it can be concluded that because of the geometry and the boundary conditions of the problem, the resultant complex pressure field is affected by many detailed effects.

In the second animation (Online resource 2), showing the pressure field created by the 3.0-mm flattop laser pulse, the same propagation features can be observed. This includes focusing of the central portion of the wave, the opposite polarity of the inner and the outer portion of the edge wave and, because of the smaller size and more overlapping of the two field contributions, the less evident but still visible separation (decoupling) of the two contributing portions of the wave on the axis in the far field at posterior of the eye.

For smaller laser spots (1.0 mm, Online resource 3, and 0.35 mm, Online resource 4), the reasoning of the above analysis is still valid, keeping in mind the lateral reduction in the source size. In Online resource 3, the initial creation of the rarefaction is still observable, pertaining to the inner portion of the edge wave. As in the previous two cases, the compression and the rarefaction pulses travelling in the same direction (same angle) are not connected, because they originate from different spatial locations of the source.

Generally, for the two smallest source spots, the focusing of the central part is less obvious. There is less energy in the central part of the wave than in the two previous cases, in absolute as well as in relative terms. In the case of the smallest light–tissue interaction spots, the wave propagation resembles the propagation from a point force monopole

source. Based on the above analysis, one can deduce and understand why the compressional and the rarefactional part of the wave are slightly separated.

According to the above observations regarding the creation of the pressure wave at the cornea and its propagation into the interior of the eye, it can be said in general that for a larger source spot diameter:

- relatively tighter pressure wave focusing is expected,
- there is relatively less energy in the edge wave.

As mentioned in Introduction, regarding the effects on the tissue, the negative pressure is more destructive than the positive. Also, it is very important where the pressure occurs—in some tissues, the same pressure can result in an irreparable damage, while in others the lesion maybe heals by itself. For this reason, a detailed map of the peak positive and negative pressure amplitudes occurring at any time inside the eye following the photoablation of the cornea was calculated for each of the four cases under study. The peak negative pressure is directly proportional to the mechanical index (MI), a unitless number that can be used as a figure of merit for the bio-effects caused by the acoustic cavitation [13]. Our results for the peak negative pressures are scalable to MI. The scaling factor for ophthalmic applications is -0.0316/bar, using the central frequency of 10 MHz for the pressure wave used in our simulations.

The results in Figs. 1, 2, 3 and 4 allow the comparison of the individual features of the four different pressure transient sources, listed in Table 1. Each of Figs. 1, 2, 3 and 4 maps the resulting pressure peaks for one source size (diameter 6.5 mm, 3.0 mm, 1.0 mm and 0.35 mm in that order) and consists of six diagrams, of which the two central parts represent the contour plots of the maximum pressure amplitude inside the eye, negative (left-hand side, blue color shades) and positive (right-hand side, red color shades), occurring at any time during the propagation of the pressure transient. For example, in Fig. 1, showing the results for the largest source spot diameter, it can be observed that the largest amplitudes, both negative and positive, occur in the vitreous humour very near the eye lens. The scaling of the different contour plot value levels is logarithmic, which is reflected in the legend bar structure in the center of each figure.

On the two diagrams to the left (negative pressure) and to the right (positive pressure) of the contour plots, the axial dependencies of the maximum pressure amplitudes on the symmetry axis are presented, occurring at any time during the pulse propagation. The values on the abscissa are the distances from the source, scaled linearly, and the values on the ordinate are the pressure amplitudes, scaled logarithmically as in the contour plots, with the same color shades representing the same levels as in the contour plots.
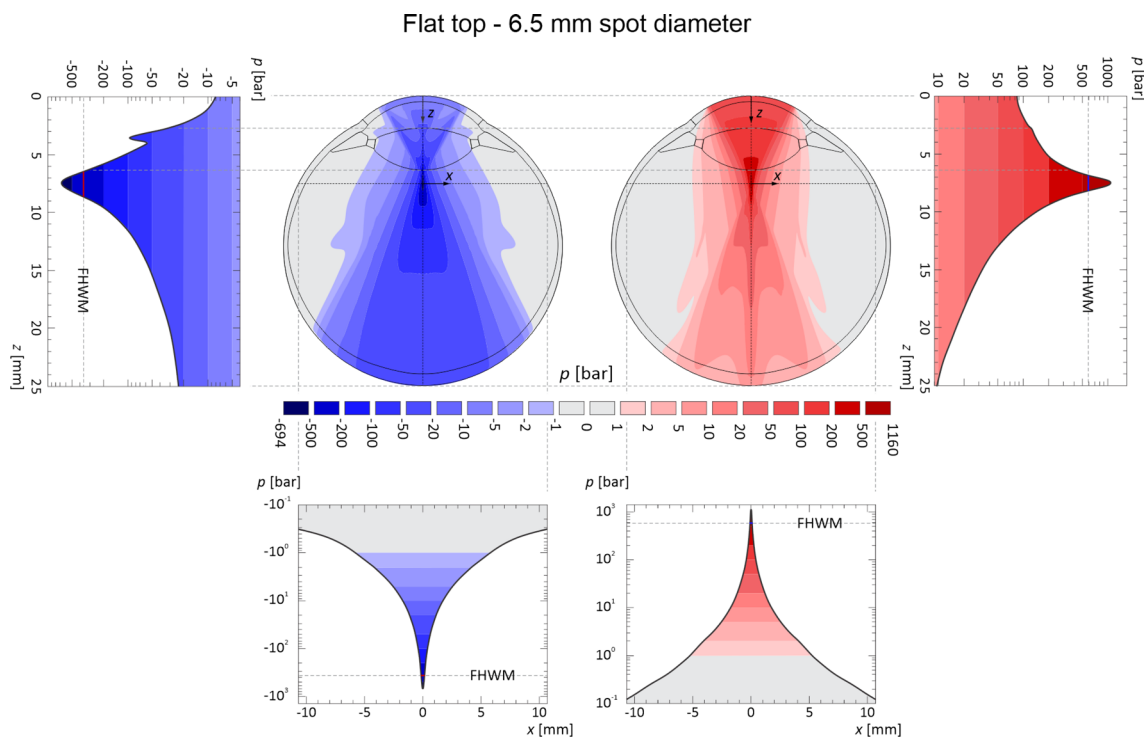
Flat top - 6.5 mm spot diameter

Fig. 1 Negative (blue) and positive (red) pressure amplitudes at any time during shock wave propagation inside the eye, source spot diameter of 6.5 mm, flattop spatial laser beam profile: contour plots (center), axial dependencies on symmetry axis (up left and right) and radial dependencies at the cross section at peak amplitude (bottom left and right). Use the factor -0.0316/bar to transform the negative pressure amplitude to the MI

The dotted horizontal lines at approximately $z=3$ mm and $z=6$ mm, extending across both the contour plots and both the diagrams, represent the position of the anterior and posterior surface of the eye lens on the symmetry axis and help the observer to compare the four different cases presented. Namely, the spatial positions of the peak pressure amplitudes are different for the four different cases:

- for the largest source diameter (6.5 mm), the largest pressure amplitudes, both negative (-694 bar) and positive (1160 bar), occur at $z=7.5$ mm from the source, which is a little over a millimeter into the vitreous humour and very near the posterior surface of the eye lens,
- for the 3.0-mm-diameter source, the positive (304 bar) peak pressure amplitude is at $z=7.0$ mm, while the negative (-201 bar) is at $z=6.0$ mm, on the posterior surface of the eye lens,
- for the two smallest diameter sources (1.0 mm and 0.35 mm), the positive peak amplitudes occur at the source (172 bar), while the peak negative pressures of -60 bar take place at about $z=1.2$ mm for the 1.0-mm source and of -43 bar around $z=0.3$ mm for the 0.35-mm source.

The vertical dotted lines in the two diagrams showing the axial dependence of the peak pressure amplitudes depict the position of the FWHM (full width at half maximum) pressure value on each diagram (red line inside the blue fill, blue line inside the red fill). Since the scaling is logarithmic, the position and the width of the FWHM value are not easily intuitively recognized. The analysis suggests that the focus for the larger source is sharper than for the smaller one, analogous to the optics case.

The bottom two diagrams in each of Figs. 1, 2, 3 and 4 show the radial dependence of the same data, at the axial position where the axial peak amplitude occurs, which is different for every case. The position is shown by the dotted vertical lines, connecting the diagram borders to the respective positions on the contour plots. Here again, the horizontal dotted lines in the two diagrams depict the position of the FWHM, in the same manner as in the axial dependence diagrams. The peaks here appear much sharper compared to the peaks in axial direction, in all four cases. Partly, this can be attributed to the axial symmetry of the model since the contributions add up constructively on the symmetry axis. In reality, the eye is not perfectly symmetric and the effect should be less pronounced.
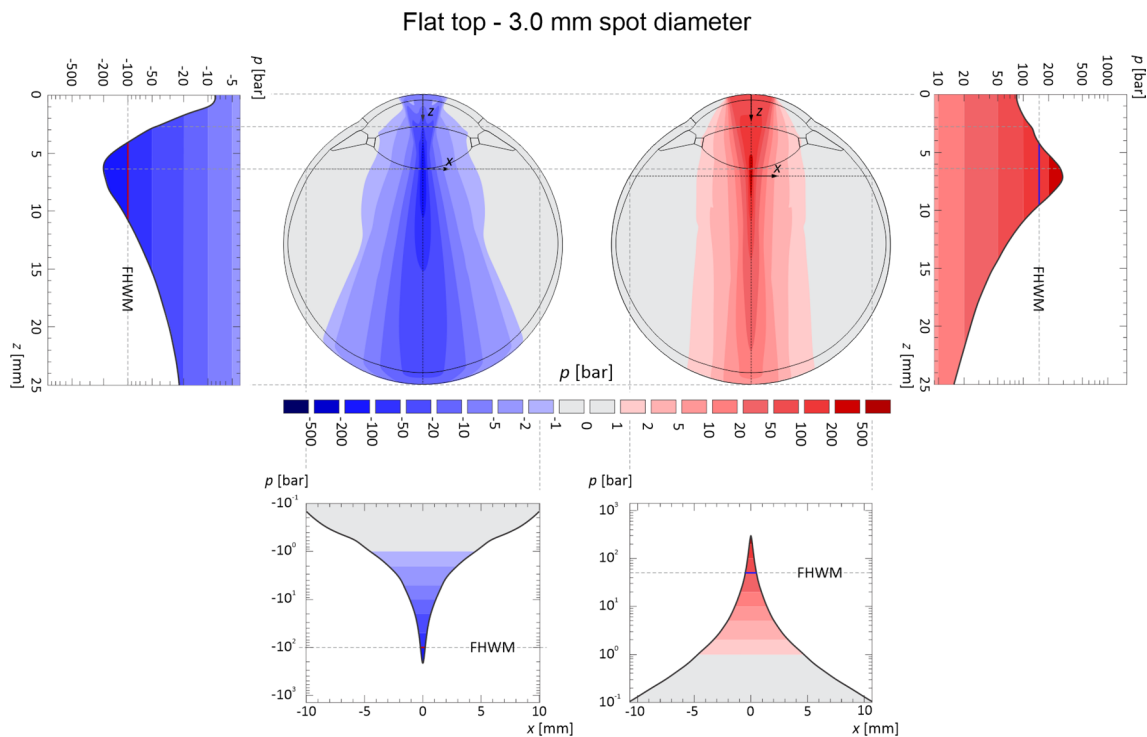
Flat top - 3.0 mm spot diameter

Fig. 2 Negative (blue) and positive (red) pressure amplitudes at any time during shock wave propagation inside the eye, source spot diameter of 3.0 mm, flattop spatial laser beam profile: contour plots (center), axial dependencies on symmetry axis (up left and right) and radial dependencies at the cross section at peak amplitude (bottom left and right). Use the factor -0.0316/bar to transform the negative pressure amplitude to the MI

Table 2 summarizes the peak positive pressure (max. pressure), peak negative pressure (min. pressure) and MI values and their respective FWHM values in the axial and radial directions for the four cases. The data on FWHM values are consistent with the fact known from optics, namely that the focus of a wide beam is tighter, i.e., has a smaller cross section compared to the focal cross section of a smaller beam. This can be observed by comparing the FWHM values in the radial direction of the 6.5-mm and the 3.0-mm beams, both for the minimum (0.32 mm vs. 0.43 mm, respectively) and for the maximum pressure (0.19 mm vs. 0.99 mm, respectively). On the other hand, the pressure field of the smallest beam (0.35 mm, Fig. 4) exhibits characteristics of propagation from a point source, having the smallest diameter at the origin. Lastly, the pressure field of the 1.0 mm beam is, regarding the shape of the focal zone, in the intermediate, transition region between the tight focusing and the point source limit. One should keep in mind that although the language of optics is used here extensively, the discussion is about the acoustics, i.e., pressure wave propagation.

It follows from the above analysis that for the large beam diameters, substantial negative and positive pressures are still present even relatively far away from the laser–tissue interaction site. An ophthalmologist has to be aware that an initial acoustic pulse which might erroneously be expected to have low amplitude, because it had already propagated for a few centimeters, can become the source of unwanted damage to the tissue far away from the source due to the described focusing effects. Assessment of the position and value of high pressure amplitudes, positive and negative, following photoablation of the corneal tissue should therefore contribute substantially in the search for improvement in medical treatments safety.
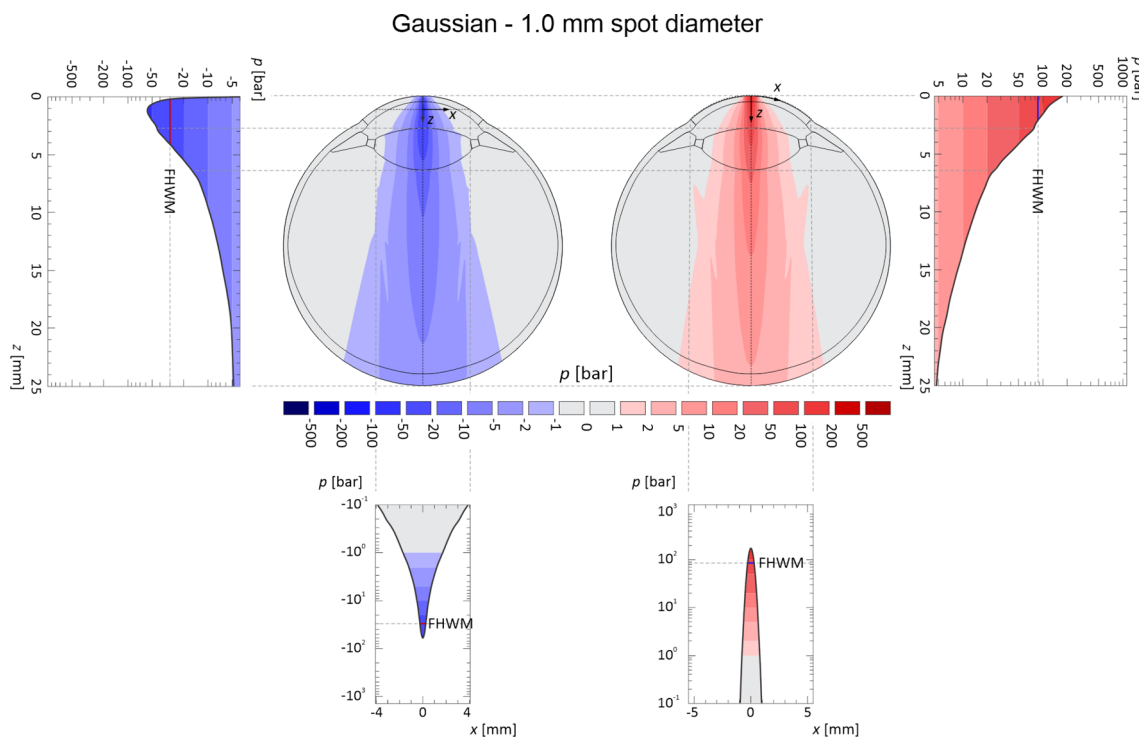
Gaussian - 1.0 mm spot diameter

Fig. 3 Negative (blue) and positive (red) pressure amplitudes at any time during shock wave propagation inside the eye, source spot diameter of 1.0 mm, Gaussian spatial laser beam profile: contour plots (center), axial dependencies on symmetry axis (up left and right) and radial dependencies at the cross section at peak amplitude (bottom left and right). Use the factor − 0.0316/bar to transform the negative pressure amplitude to the MI

5 Conclusion

The evolution of a pressure wave propagating inside a human eye, following photoablation of the human cornea, was analyzed for four typical laser beams that are clinically employed in contemporary LASIK/PRK ophthalmic procedures. The 6.5-mm-diameter flattop beam corresponds to the widest available broad beam, the 3.0-mm-diameter flattop beam corresponds to the medium size, aperture spatially modulated broad beam, and the 1.0-mm-diameter Gaussian beam relates to the typical flying spot beam. All these laser beams are produced by ArF excimer lasers operating at 193 nm, while the very small 0.35-mm-diameter Gaussian beam is a typical fifth harmonic output of the diode-pumped solid-state lasers emitting light in the interval between 208 and 213 nm.

The calculated animations give a spatiotemporal insight into the dynamics of the transient pressure wave. Depending on the beam spot on the cornea, the wave pattern resembles a field similar to the pattern of the piston source if the beam is large and to the point source if the beam is very small. Various physical effects, such as propagation, wave reflection, attenuation, focusing, phase shift, to name the most importance ones, have to be taken into account to properly describe the dynamics of the pressure pulse.

For each laser pulse, the contour plots of the peak positive and peak negative pressure amplitudes give a timeless representation of the maximum compressive and tensile loading of ocular tissues. The comparative analysis of these pressure contour plots as well as the corresponding diagrams of the axial and radial peak pressure values is expected to be of substantial help to medical professionals. Based on the presented results, they can assess the critical parameters influencing photoablation that give rise to potentially problematic conditions regarding the positive and negative pressure values inside the eye which exceed the limits, considered safe for the patient.
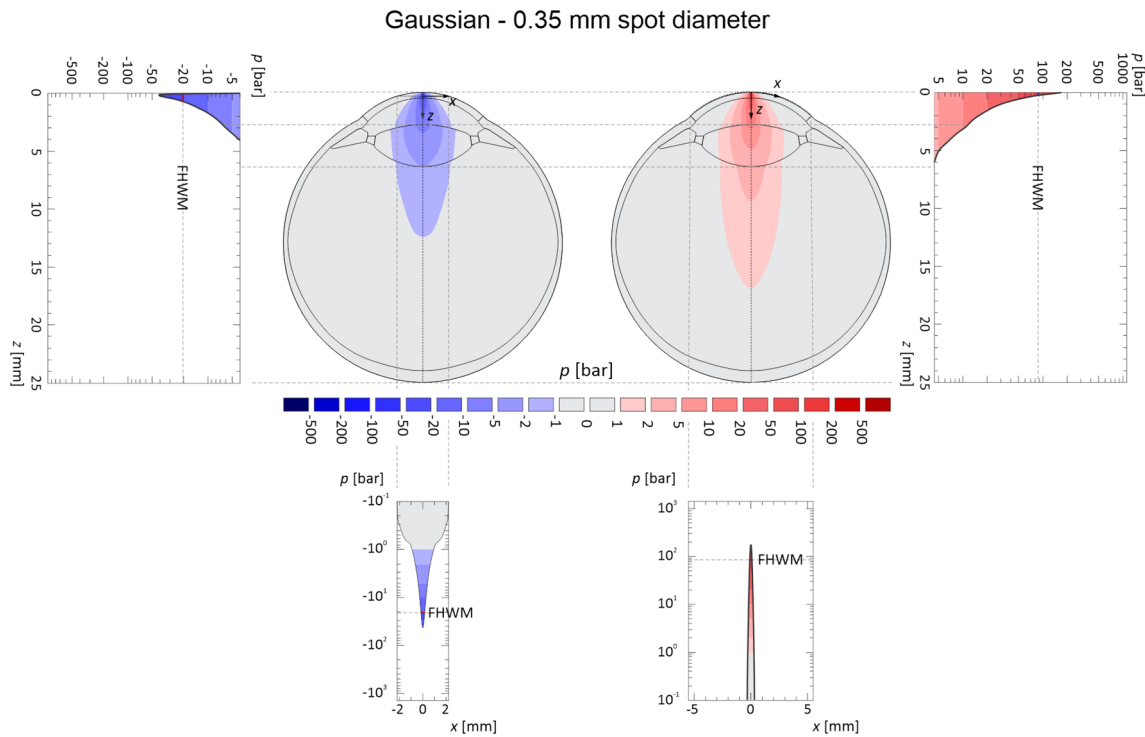
Gaussian - 0.35 mm spot diameter

Fig. 4 Negative (blue) and positive (red) pressure amplitudes at any time during shock wave propagation inside the eye, source spot diameter of 0.35 mm, Gaussian spatial laser beam profile: contour plots (center), axial dependencies on symmetry axis (up left and right) and radial dependencies at the cross section at peak amplitude (bottom left and right). Use the factor -0.0316/bar to transform the negative pressure amplitude to the MI

Table 2 The calculated peak values of minimum and maximum pressure and MI, and the respective FWHM values in the axial and radial direction, for the four beam types

Beam type	Min. pressure (bar)	MI at 10 MHz	Max. pressure (bar)	FWHM—min. pressure (mm)		FWHM—max. pressure (mm)	
				Axial	Radial	Axial	Radial
Flattop—6.5 mm	− 694	21.9	1160	2.19	0.32	1.36	0.19
Flattop—3.0 mm	− 201	6.36	304	6.70	0.43	5.36	0.99
Gaussian—1.0 mm	− 60	1.9	172	3.93	0.51	2.07	0.59
Gaussian—0.35 mm	− 43	1.4	172	0.68	0.33	0.25	0.21

References

1. D.T. Azar, *Refractive Surgery E-Book* (Elsevier, Amsterdam, 2019)
2. M. El Bahrawy, J.L. Alió, Eye Vis. **2**, 6 (2015)
3. T. Požar, M. Halilovič, D. Horvat, R. Petkovšek, Appl. Phys. A **124**, 112 (2018)
4. E.-A. Brujan, A. Vogel, J. Fluid Mech. **558**, 281 (2006)
5. J. Coleman, M. Whitlock, T. Leighton, J.E. Saunders, Phys. Med. Biol. **38**, 1545 (1993)
6. T. Lee, J.G. Ok, L.J. Guo, H.W. Baac, Appl. Phys. Lett. **108**, 104102 (2016)
7. T.-B. Fan, J. Tu, L.-J. Luo, X.-S. Guo, P.-T. Huang, D. Zhang, Chin. Phys. Lett. **33**, 084302 (2016)
8. U.S. Food and Drug Administration, List of FDA-Approved Lasers for LASIK, updated 6. Sept 2018.
9. U.S. Food and Drug Administration, FDA-Approved Lasers for PRK and Other Refractive Surgeries, updated 3. Dec 2019.
10. T. Požar, D. Horvat, B. Starman, M. Halilovič, R. Petkovšek, J. Appl. Phys. **125**, 204701 (2019)
11. S. Siano, R. Pini, F. Rossi, R. Salimbeni, P.G. Gobbi, Appl. Phys. Lett. **72**, 647 (1998)

12. R.R. Krueger, T. Seiler, T. Gruchman, M. Mrochen, M.S. Berlin, Ophthalmology **108**, 1070 (2001)

13. F.A. Duck, A.C. Baker, H.C. Starritt, *Ultrasound in Medicine* (CRC Press, Boca Raton, 1998)

14. E. Spörl, T. Gruchmann, U. Genth, P. Mierdel, T. Seiler, Ophthalmol. Z. Dtsch. Ophthalmol. Ges. **94**, 578 (1997)

15. O. Kermani, H. Lubatschowski, Fortschritte Ophthalmol. Z. Dtsch. Ophthalmol. Ges. **88**, 748 (1991)

16. D.T. Azar, D.D. Koch (eds.), *LASIK: Fundamentals, Surgical Techniques, and Complications* (Marcel Dekker, New York, 2003)

17. G.C. Everstine, Comput. Struct. **65**, 307 (1997)

18. A. Freedman, J. Sound Vib. **170**, 495 (1994)